HTML ABSTRACT + LINKS

JOURNAL OF APPLIED PHYSICS **97**, 123705 (2005)

Thermoelectric effects in wurtzite GaN and $Al_xGa_{1-x}N$ alloys

Weili Liu[a] and Alexander A. Balandin
Nano-Device Laboratory,[b] Department of Electrical Engineering, University of California - Riverside, Riverside, California 92521

(Received 4 March 2005; accepted 6 April 2005; published online 20 June 2005)

We have investigated theoretically the thermoelectric effects in wurtzite GaN crystals and $Al_xGa_{1-x}N$ alloys. The electron-transport model includes all dominant energy-dependent electron-scattering mechanisms, such as charged dislocation and ionized impurity scattering, polar optical phonon, deformation potential, and piezoelectric acoustic-phonon scattering. The results of the calculation show that GaN-based alloys may have some potential as thermoelectric materials at high temperature. It was found that the thermoelectric figure-of-merit for bulk GaN at $T=300$ K is about 0.0017 while it can reach 0.2 in the thermally resistive $Al_{0.4}Ga_{0.6}N$ alloy at $T=1000$ K. The obtained results agree well with available experimental data. The developed calculation procedure can be used for the optimization of the thermoelectric properties of GaN alloys. The proposed integration of the GaN high-power microwave and optoelectronic devices with the active thermoelectric cooling implemented on the same material system can improve the device performance. © *2005 American Institute of Physics*. [DOI: 10.1063/1.1927691]

I. INTRODUCTION

Wide band-gap nitride semiconductors are very promising for high-power density high-temperature applications in microwave communications, power electronics, and optoelectronics.[1–4] In addition to their wide band gap, these materials also demonstrate excellent electronic transport properties. For example, the sheet carrier density of the two-dimensional electron gas (2DEG) formed at the AlGaN/GaN interface can be higher than 10^{13} cm^{-2}, and the electron mobility for such a high-density 2DEG can be as large as 2000 cm^2/V s at room temperature.[5,6] Great progress has been achieved in GaN-based microwave technology. GaN transistors with very high breakdown voltage,[7] high output-power level,[8] and low flicker noise[9,10] have been demonstrated.

The envisioned optical, optoelectronic, and electronic applications of GaN and related compounds crucially depend on the effectiveness of heat removal from the device active areas.[11] Due to the very high power densities involved and continuing downscaling trend, one has to come up with an efficient thermal management approach for GaN-based devices. An integrated thermoelectric spot cooling has been proposed earlier for optoelectronic and electronic devices as a way to improve their performance.[12] For the devices based on GaN-related materials and with more severe cooling requirement, the integrated spot cooling can become a possible solution to the thermal challenges. Apparently, the preferred thermoelectric material, in terms of integration, for the proposed cooling system should also be based on GaN. To realize this, the high-efficiency GaN-based thermoelectric elements have to be developed. The latter provides a strong motivation for research aimed at understanding the thermoelectric effects in GaN and GaN-related alloys.

There has been very little experimental work done on the thermoelectric properties of GaN and its alloys.[13–15] To the best of our knowledge, no theoretical analysis of the thermoelectric properties of GaN material has ever been reported. The preliminary experimental data reported for bulk GaN, InN and AlInN, AlGaInN alloys show some promise. The thermoelectric figure-of-merit $ZT=S^2\sigma T/K$ value of 0.1 has been achieved at 873 K.[15] Here S is the Seebeck coefficient, σ is the electrical conductivity, K is the thermal conductivity, and T is the absolute temperature. For comparison, the ZT values of the best commercial thermoelectric material such as the Bi_2Te_3 alloy is about 0.7–0.9 at room temperature.[16] Obviously, the reported ZT values for GaN need further enhancement to have a chance in competing even for the GaN-based device spot-cooling applications. A detailed theoretical study of the thermoelectric properties of wurtzite GaN and its alloys would be of great help to determine the possible ways for ZT improvement.

Despite a large body of work conducted on electron transport in bulk GaN and its heterostructures,[17–22] the thermoelectric effects have not been considered theoretically yet. In this paper we present a theoretical study of the thermoelectric characteristics of wurtzite GaN crystals and related materials. The electron-transport model includes all dominant energy-dependent electron-scattering mechanisms, such as dislocation and ionized impurity scattering, polar optical-phonon scattering, deformation potential, and piezoelectric acoustic-phonon scattering. The lattice thermal conductivity is calculated using the virtual-crystal model[23,24] validated with available experimental data.

The remainder of the paper is organized as follows. Section II describes the electron-transport model and discusses the contributions of various scattering mechanisms to the electron mobility degradation in GaN. The results of the modeling of the thermoelectric properties of GaN crystals are presented in Sec. III. We give our conclusions in Sec. IV.

[a]Electronic mail: weili@ee.ucr.edu
[b]Website address: http://ndl.ee.ucr.edu/

 © 2005 American Institute of Physics

Downloaded 25 Jun 2005 to 138.23.226.121. Redistribution subject to AIP license or copyright, see http://jap.aip.org/jap/copyright.jsp

II. ELECTRON TRANSPORT IN GAN

The purpose of this paper is to theoretically analyze the thermoelectric properties of the GaN material. The thermoelectric figure-of-merit ZT is defined as

$$ZT=\frac{S^2\sigma}{k_e+k_{\mathrm{ph}}}T, \tag{1}$$

where S is the Seebeck coefficient, σ is the electrical conductivity, k_e is the electronic thermal conductivity, k_{ph} is the lattice thermal conductivity, and T is the absolute temperature. The power factor $S^2\sigma$ characterizes the electronic energy-conversion ability of the given material. In Eq. (1), S, σ, and k_e are determined by the electron-transport properties.

In this study, we focus on the n-type GaN. The analysis for p-type materials is similar. We model the electron transport in GaN by solving the Boltzmann transport equation with the relevant energy-dependent electron-scattering terms. In the presence of an external field $\vec{P}$ and temperature gradient ∇T, the electron distribution function can be described by the Boltzmann transport equation[25]

$$\vec{v}\cdot\frac{\partial f}{\partial \vec{r}}+\frac{e\vec{P}}{\hbar}\cdot\frac{\partial f}{\partial \vec{k}}=-\left(\frac{\partial f}{\partial t}\right)_{\mathrm{coll}}, \tag{2}$$

where $\vec{v}$ is the electron velocity, $\vec{P}$ is the external electric field, f is the electron distribution function, k is the electron wave vector, e is the electron charge, and $\hbar$ is Plank's constant. The notations $\partial/\partial\vec{r}$ and $\partial/\partial\vec{k}$ are used for the derivatives in the real space and k space, respectively. The collision term $\partial f/\partial t|_c$ includes all relevant electron relaxation mechanisms for a given material. Solving the Boltzmann equation using the standard procedure,[25] one can express the electron distribution function f through the equilibrium Fermi distribution function f_0, i.e.,

$$f(k)=f_0(k)+\tau_{\mathrm{tot}}(k)\left(-\frac{\partial f_0(k)}{\partial E}\right)\vec{v}\left[-e\vec{P}-\nabla\varsigma-\frac{E-\varsigma}{T}\nabla T\right]. \tag{3}$$

Here $E=(\hbar^2k^2/2m_{\mathrm{eff}})$ is the electron energy and ς is the Fermi energy. The energy-dependent relaxation time $\tau_{\mathrm{tot}}(k)$ is given by Matthiessen's rule as

$$\tau_{\mathrm{tot}}{}^{-1}(k)=\sum\tau_i^{-1}(k), \tag{4}$$

where the index i represents each relevant scattering term.

Different electron-scattering mechanisms and their respective contributions are usually manifested in the mobility dependence on temperature, doping density, and defect concentrations. The low-field electron mobility in bulk GaN, AlGaN, and GaN/AlGaN heterostructures has been investigated both theoretically and experimentally by many research groups.[17–22] The spatial separation of ionized donors from two-dimensional electron gas (2DEG) in GaN/AlGaN heterostructures allows one to achieve relatively high mobility values, often above $1000\ \mathrm{cm^2/V\,s}$ at room temperature.[6,17] The use of the high-Al content barriers was another approach taken to increase mobility while maintaining a high sheet carrier-concentration density of $n_e \sim 10^{13}\ \mathrm{cm^{-2}}$.[26] However, the reported mobility data for bulk GaN display strong discrepancy in both absolute values and temperature dependence.[18,19] The dominant mechanisms of electron scattering in GaN are still subjects of debates. Katz *et al.*[17] suggested that the polar optical-phonon scattering is the dominant term, rather than the acoustic-phonon scattering considered by Knap *et al.*[20] Look and Sizelove[19] indicated that the charged dislocation scattering could play a major role in limiting the electron mobility. To a large extent, the question of the dominant term depends on the material's quality and actual concentration of the defects and doping densities.

Based on previous studies, we consider five major scattering terms to the Boltzmann transport equation. The first one is the charged dislocation scattering. The time constant for this mechanism is given by[19]

$$\tau_{\mathrm{dis}}(k)=\frac{\hbar^3\varepsilon_s^2c^2}{N_{\mathrm{dis}}m_{\mathrm{eff}}e^4}\frac{(1+4\lambda_D^2k_\perp^2)^{3/2}}{\lambda_D^4}, \tag{5}$$

where ε_s is the static dielectric constant, c is the lattice constant along the (0001) direction, m_{eff} is the effective mass, N_{dis} is the dislocation density, $k_\perp$ is the component of electron wave-vector k perpendicular to the direction of dislocation, and λ_D is the Debye length defined as

$$\lambda_D=\sqrt{\frac{\kappa_B T\varepsilon_s}{e^2 n}}, \tag{6}$$

where κ_B is Boltzmann's constant and n is the free-electron density, which can be determined from the charge balance equation

$$n+N_A+\frac{N_{\mathrm{dis}}}{c}=\frac{N_D}{1+\dfrac{gn}{N_c}\exp\left(\dfrac{E_D}{\kappa_B T}\right)}. \tag{7}$$

Here N_A is the acceptor concentration, N_D is the donor concentration, $g(=2)$ is the degeneracy of the electronic state, N_C is the effective density of states, and E_D is the donor activation energy. In our calculations, we assume $N_A=10^{15}\ \mathrm{cm^{-3}}$ and $E_D=29$ meV (Ref. 27).

The second considered mechanism is the ionized impurity scattering. The electron-scattering rate for this mechanism can be written as[28]

$$\frac{1}{\tau_{\mathrm{imp}}(k)}=\frac{\pi^{3/2}Z^2e^4N_{\mathrm{imp}}[\ln(1+b)-b/(1+b)]}{2^{7/2}m_{\mathrm{eff}}^{1/2}(4\pi\varepsilon_s)^2(\kappa_B T)^{3/2}}, \tag{8}$$

where N_{imp} is the ionized impurity density, $Z(=1)$ is the charge number of the ionized atom. The Brooks–Herring parameter b is given by

$$b=\frac{24m_{\mathrm{eff}}\varepsilon_s(\kappa_B T)^2}{ne^2\hbar^2}. \tag{9}$$

Three other relaxation processes are related to scattering on phonons. Their scattering mechanisms and momentum relaxation times have been discussed in many literatures, and

Downloaded 25 Jun 2005 to 138.23.226.121. Redistribution subject to AIP license or copyright, see http://jap.aip.org/jap/copyright.jsp

the formula are well described in textbooks.[29] The deformation-potential acoustic phonon scattering rate is written as

$$\frac{1}{\tau_{\rm def}(k)} = \frac{\Xi_D^2 \kappa_B T (2m_{\rm eff})^{3/2}\sqrt{E}}{4\pi\hbar^4 c_{\rm LA}}, \tag{10}$$

where Ξ_D is the deformational potential, and $c_{\rm LA}$ is the angular average of the elastic constant for longitudinal acoustic (LA) phonon modes. The piezoelectric acoustic phonon scattering rate is given by

$$\frac{1}{\tau_{\rm pe}(k)} = \frac{e^2 K_{\rm av}^2 \kappa_B T}{2\pi\varepsilon_s \hbar^2 \upsilon}\left[1 + \frac{1}{1+8m_{\rm eff}E/\hbar^2 q_s^2} - \frac{\hbar^2 q_s^2}{4m_{\rm eff}E} \times \log\left(1+\frac{8m_{\rm eff}E}{\hbar^2 q_s^2}\right)\right]. \tag{11}$$

Here υ is the electron group velocity. $K_{\rm av}$ is the electromechanical coupling factor defined by the expression

$$K_{\rm av}^2 = \frac{\langle e_{\rm LA}^2\rangle}{\varepsilon_s c_{\rm LA}} + \frac{\langle e_{\rm TA}^2\rangle}{\varepsilon_s c_{\rm TA}}, \tag{12}$$

where $c_{\rm TA}$ is the angular average of the elastic constant for transverse acoustic (TA) phonon modes. The piezoelectric tensor for wurtzite GaN can be explicitly written as[30]

$$\overleftrightarrow{e} = \begin{pmatrix} 0 & 0 & 0 & 0 & e_{15} & 0 \\ 0 & 0 & 0 & e_{15} & 0 & 0 \\ e_{31} & e_{31} & e_{33} & 0 & 0 & 0 \end{pmatrix}. \tag{13}$$

The spherical square averages of the piezoelectric constants for LA and TA phonon modes are given by the expressions

$$\langle e_{\rm LA}^2\rangle = \frac{8(2e_{15}+e_{31})^2}{105} + \frac{4}{35}(2e_{15}+e_{31})e_{33} + \frac{e_{33}^2}{7}, \tag{14}$$

$$\langle e_{\rm TA}^2\rangle = \frac{2}{35}(e_{33}-e_{15}-e_{31})^2 + \frac{16}{105}(e_{33}-e_{15}-e_{31})e_{15} + \frac{16}{35}e_{15}^2. \tag{15}$$

The reciprocal of the screening length, q_s, is given by

$$q_s^2 = -\frac{e^2}{\varepsilon_s}\int \frac{df_0(E)}{dE} N(E)dE. \tag{16}$$

Finally, the last relaxation term included in our calculations is the polar optical-phonon scattering. The scattering rate for this type of process is given as[21]

$$\frac{1}{\tau_{\rm lo}(k)} = W_0[n(\omega)+1]\frac{f_0(E+\hbar\omega)}{f_0(E)}\left(\frac{\hbar\omega}{E}\right)^{1/2} \times \sinh^{-1}\left(\frac{E}{\hbar\omega}\right)^{1/2}, \tag{17}$$

where ω is the optical-phonon frequency, $n(\omega)$ is the Boson factor, and

$$W_0 = \frac{e^2}{4\pi\hbar}\left(\frac{2m_{\rm eff}\omega}{\hbar}\right)^{1/2}\left(\frac{1}{\varepsilon_\infty} - \frac{1}{\varepsilon_s}\right). \tag{18}$$

For the total relaxation time and for each of its components, one can define the average relaxation time[31]

$$\langle\tau\rangle = \frac{\int \tau(E) E \frac{df(E)}{dE} dE}{\int E \frac{df(E)}{dE} dE} \tag{19}$$

and calculate the electron mobility defined as

$$\mu = \frac{e\langle\tau\rangle}{m_{\rm eff}}. \tag{20}$$

The thermoelectric characteristics σ, S, and k_e are derived from the solution of the Boltzmann equation and written as[32]

$$\sigma = e^2 \int \left(-\frac{\partial f_0}{\partial E}\right)\tau_{\rm tot}(k)\upsilon^2(k)\frac{dk^3}{4\pi^3}, \tag{21}$$

$$S = -\frac{1}{\sigma}\frac{e}{T}\int \left(-\frac{\partial f_0}{\partial E}\right)\tau_{\rm tot}(k)\upsilon^2(k)(E-\varsigma)\frac{dk^3}{4\pi^3}, \tag{22}$$

$$k_e = \frac{e}{T^2}\int \left(-\frac{\partial f_0}{\partial E}\right)\tau_{\rm tot}(E)\upsilon^2(k)(E-\varsigma)^2\frac{dk}{4\pi^3} - \sigma S^2 T. \tag{23}$$

The dependence of the phonon contribution $k_{\rm ph}$ to the thermal conductivity [see Eq. (1)] on the dislocation and point defect densities has been studied in detail by Zou and co-workers.[33,34] It has been established that the room-temperature thermal conductivity in wurtzite GaN is sensitive to the dislocation line density $N_{\rm dis}$ only for very large values of $N_{\rm dis} > 5\times 10^{10}$ cm^{-2} (Ref. 33). At this high dislocation range the variation of the dislocation line density by two orders of magnitude can bring about a large, factor of two, variation in the thermal conductivity value. For GaN materials with lower dislocation density, the room-temperature thermal conductivity is more sensitive to the concentration of point defects (impurities, dopants, etc.). For example, the change in the doping density can lead to a variation of $k_{\rm ph}$ from 1.77 W/cm K to 0.86 W/cm K at 300 K.[34] In this work we selected $N_{\rm dis} \leqslant 5\times 10^{10}$ cm^{-2} and determine $k_{\rm ph}$ from the virtual-crystal model.[23,24] One should point out here that the $k_{\rm ph}$ term is much larger than k_e for most practical situations even at very large doping density.[33] In our calculations, the GaN material constants, except for piezoelectric constants, are taken from Ref. 35. The piezoelectric constants were estimated to be $e_{15}=e_{31}=-0.42$ C/m^2 and $e_{33}=0.72$ C/m^2 (Refs. 35 and 36).

III. RESULTS AND DISCUSSION

As stated before, different electron-scattering mechanisms and their relative contributions are displayed in the mobility dependence on temperature, doping density, and defect concentrations. The relative importance of each specific scattering mechanism varies sensitively with different $N_{\rm dis}$, N_D, and temperature. To demonstrate this, we show six plots of the electron mobility in n-type GaN as a function of the carrier density at different temperatures and $N_{\rm dis}$ in Figs. 1 and 2. The dislocation densities in Figs. 1 and 2 are 5×10^{10} and 5×10^6 cm^{-2}, respectively. The temperatures in

Downloaded 25 Jun 2005 to 138.23.226.121. Redistribution subject to AIP license or copyright, see http://jap.aip.org/jap/copyright.jsp

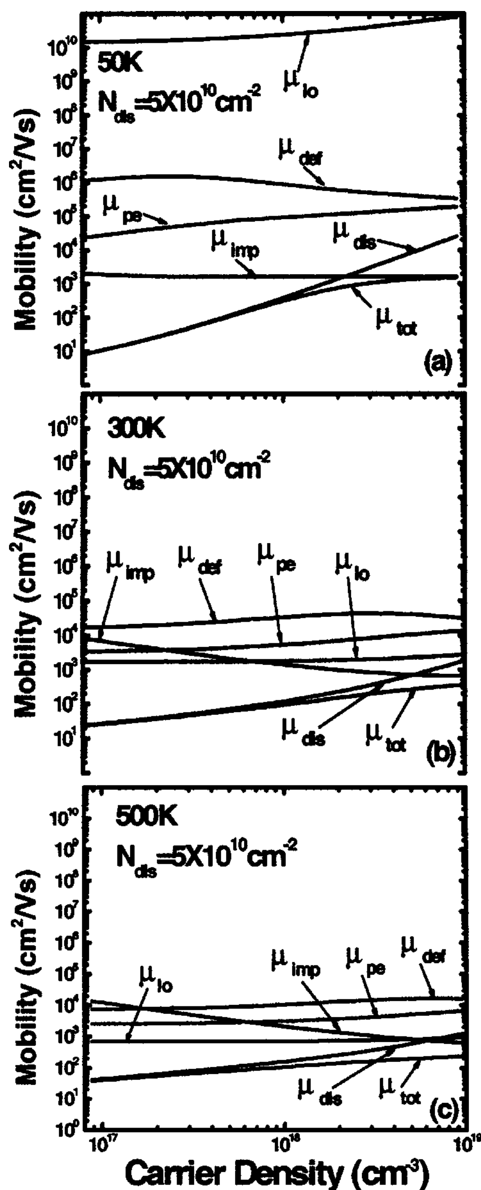

FIG. 1. Total mobility and partial mobility components as functions of the carrier density for $N_{\mathrm{dis}}=5\times10^{10}$ cm^{-2} at (a) $T=50$ K, (b) $T=300$ K, and (c) $T=500$ K.

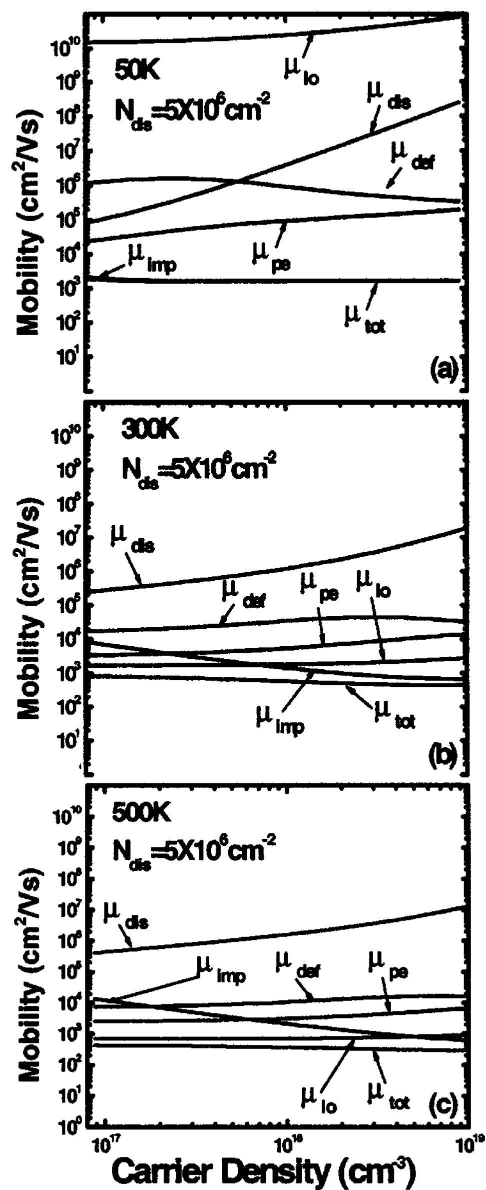

FIG. 2. Total mobility and partial mobility components as functions of the carrier density for $N_{\mathrm{dis}}=5\times10^{6}$ cm^{-2} at (a) $T=50$ K, (b) $T=300$ K, and (c) $T=500$ K.

Figs. 1(a) and 2(a), Figs. 1(b) and 2(b), and Figs. 1(c) and 2(c) are 50, 300, and 500 K, respectively. The carrier density n is nearly proportional to N_D when $n \gg 10^{15}$ cm^{-3}. In each plot, the total mobility and partial mobilities limited by a specific scattering mechanism are indicated with different symbols. It can be seen that when N_{dis} is high, the mobility is limited by either the charged dislocation mobility μ_{dis} at low N_D or by both the ionized impurity and charged dislocation mobilities $\mu_{\mathrm{imp}}+\mu_{\mathrm{dis}}$ at high N_D. In this case, the absolute value of the mobility decreases appreciably with N_{dis} increase. When N_{dis} is low, the mobility is dominated by the ionized impurity and piezoelectric mobilities $\mu_{\mathrm{imp}}+\mu_{\mathrm{pe}}$ at low temperature and by the ionized impurity and longitudinal optical (LO) phonon mobilities $\mu_{\mathrm{imp}}+\mu_{\mathrm{lo}}$ at high temperature.

One of the specifics of the GaN material is that it comes with very large variation of the dislocation densities. Uniquely enough, GaN-based devices operate at dislocation densities at which devices based on other material systems fail. The optimization of thermoelectric materials usually requires rather high doping density to raise the Fermi level to a desired position.[16] In this situation, N_{dis} becomes a rather important additional parameter for tuning the material properties. In the following analysis, we focus on the effects of the dislocation scatterings on thermoelectric properties.

Figure 3 shows the variation of the mobility with temperature for $N_{\mathrm{dis}}=5\times10^{6}$ cm^{-2} (squares), $N_{\mathrm{dis}}=5\times10^{8}$ cm^{-2} (circles), and $N_{\mathrm{dis}}=5\times10^{10}$ cm^{-2} (triangles) at the constant doping density $N_D=5\times10^{19}$ cm^{-3}. As will be shown later, the value $N_D=5\times10^{19}$ cm^{-3} is close to the optimum doping level for ZT at 300 K. A peak in the mobility curve and a decrease of the mobility with temperature is observed for $N_{\mathrm{dis}}=5\times10^{6}$ cm^{-2} and $N_{\mathrm{dis}}=5\times10^{8}$ cm^{-2}. The curve for $N_{\mathrm{dis}}=5\times10^{10}$ cm^{-2}, on the other hand, shows a

Downloaded 25 Jun 2005 to 138.23.226.121. Redistribution subject to AIP license or copyright, see http://jap.aip.org/jap/copyright.jsp

monotonic increase of the mobility with temperature due to the dominance of the charged dislocation scattering over the optical-phonon scattering and ionized impurity scattering. Similar dependencies were reported by Look and Sizelove.[19]

Once the electron-scattering mechanisms are known, one can calculate the thermoelectric characteristics σ, S, k_e, and ZT from Eqs. (21), (22), (23), and (1), respectively. Figure 4 demonstrates the variation of (a) σ, (b) S, (c) k_e, and (d) ZT with the carrier density at 300 K at a moderate doping density of $N_{\mathrm{dis}}=5\times10^8\ \mathrm{cm}^{-2}$. In the ZT calculation, the GaN bulk lattice thermal-conductivity value is taken to be $k_{\mathrm{ph}}=173\ \mathrm{W/m\,K}$, which has been obtained from the virtual-crystal model.[24] The obtained room-temperature ZT is about 0.0017 for the carrier concentration of about $10^{19}\ \mathrm{cm}^{-3}$. To validate the model and calculation procedure, we compared our σ and S values with the only measurement data available for the thermoelectric properties of GaN reported in Ref. 13. The measured value of the electrical conductivity σ and the Seebeck coefficient S were $0.52\times10^4\ \Omega^{-1}\ \mathrm{m}^{-1}$ and $-50\ \mu\mathrm{V/K}$, respectively. Since the carrier density in the sample, at which these values were obtained, has not been reported in Ref. 13, a direct comparison is not possible. At the same time, one can see from Figs. 4(a) and 4(b) that our results are in reasonable agreement with the measured values if one assumes the carrier density around $5\times10^{18}\ \mathrm{cm}^{-3}\sim1\times10^{19}\ \mathrm{cm}^{-3}$. This indicates that the developed model provides a reasonably accurate description of the thermoelectric behavior of the bulk GaN.

Figures 5(a), 5(b), and 5(c) show the calculated σ, S, and k_e, respectively, from 0 to 1000 K with $N_D=1\times10^{19}\ \mathrm{cm}^{-3}$ at three levels of N_{dis}. The figures indicate that, when N_{dis} is larger than the certain level, σ and k_e drop appreciably with increasing N_{dis}. The Seebeck coefficient, which relatively weakly depends on the scattering mechanisms, is less affected by the difference in the dislocation scattering rate. The critical dislocation level can be estimated from

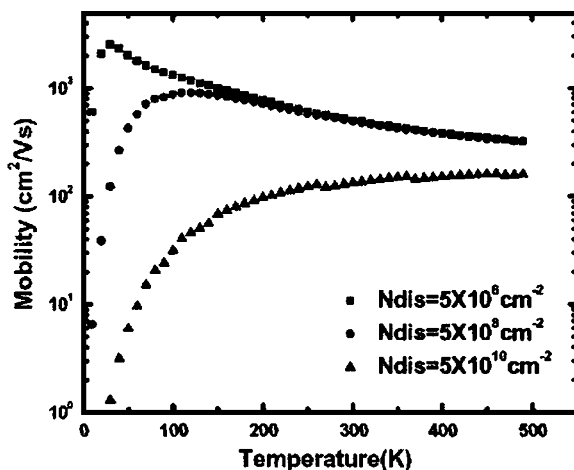

FIG. 3. Mobility as a function of temperature for $N_{\mathrm{dis}}=5\times10^6\ \mathrm{cm}^{-2}$ (squares), $N_{\mathrm{dis}}=5\times10^8\ \mathrm{cm}^{-2}$ (circles) and $N_{\mathrm{dis}}=5\times10^{10}\ \mathrm{cm}^{-2}$ (triangles) with $N_D=5\times10^{19}\ \mathrm{cm}^{-3}$.

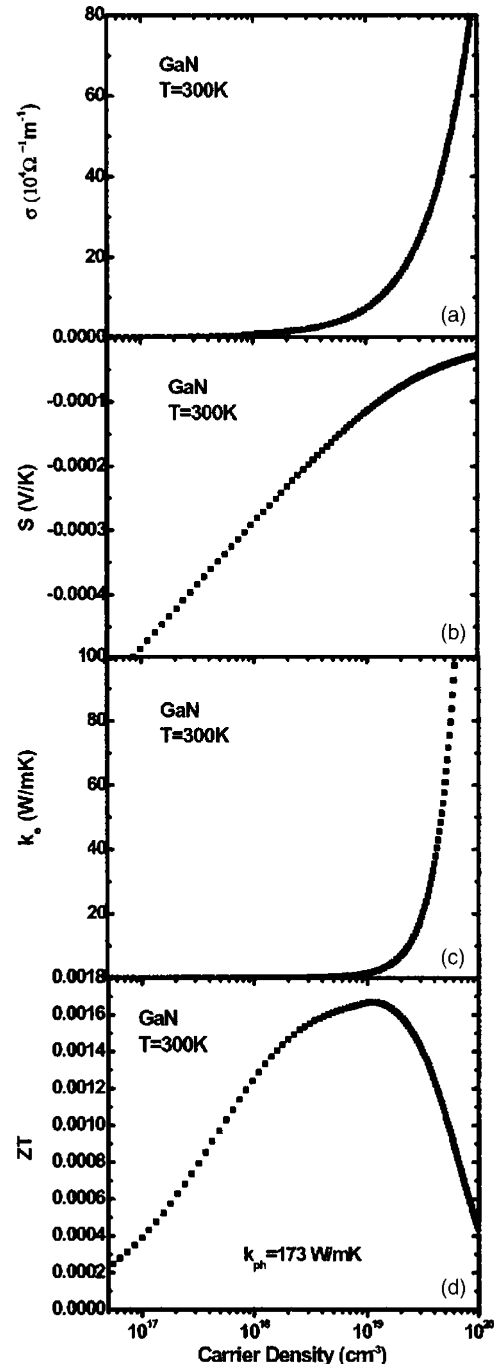

FIG. 4. Thermoelectric characteristics (a) electrical conductivity σ, (b) Seebeck coefficient S, (c) electronic contribution to the thermal conductivity k_e, and (d) thermoelectric figure-of-merit ZT as the function of the carrier density at $T=300$ K with $N_{\mathrm{dis}}=5\times10^8\ \mathrm{cm}^{-2}$. In panel (d), the thermal conductivity $k_{\mathrm{ph}}=173\ \mathrm{W/m\,K}$ calculated using the virtual-crystal model for $T=300$ K has been used (Ref. 24).

$$\tau_{\mathrm{dis}}^{-1}=\sum_i \tau_{i\ \mathrm{others}}^{-1}. \tag{24}$$

If N_{dis} is reduced below the critical level, the transport properties become relatively insensitive to the charged dislocation scattering.

Using the model described above, one can calculate the thermoelectric figure-of-merit of bulk wurtzite GaN and related alloys. According to Eq. (1), an appropriate model for lattice thermal transport is required for ZT value estimation.

Downloaded 25 Jun 2005 to 138.23.226.121. Redistribution subject to AIP license or copyright, see http://jap.aip.org/jap/copyright.jsp

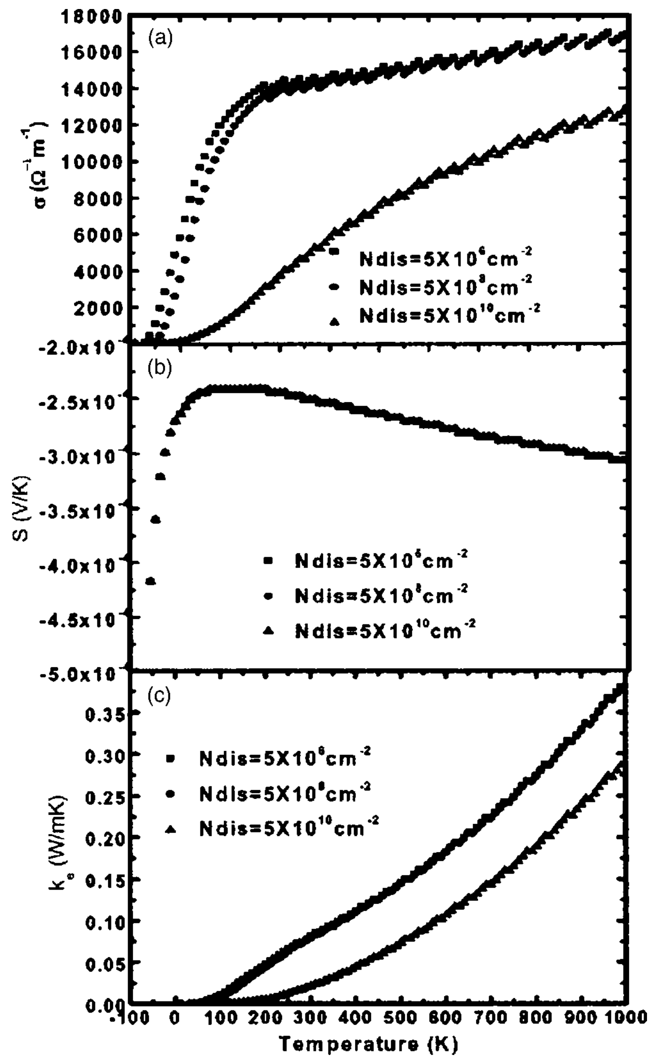

FIG. 5. Variation of (a) electrical conductivity σ, (b) Seebeck coefficient S, and (c) electronic contribution to the thermal conductivity k_e from 0 to 1000 K at $N_D = 1 \times 10^{19}$ cm^{-3} and different dislocation densities.

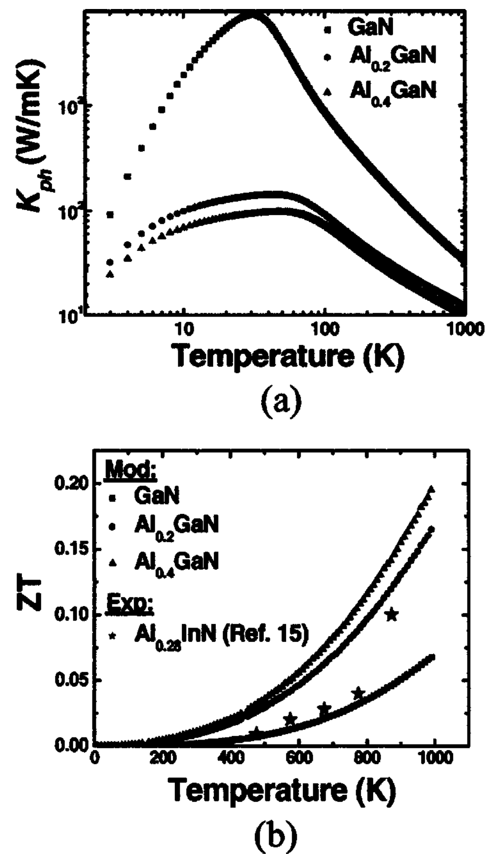

FIG. 6. (a) Lattice thermal conductivity of GaN, $Al_{0.2}Ga_{0.8}N$, and $Al_{0.4}Ga_{0.6}N$ from 0 to 1000 K calculated using the virtual-crystal model (Ref. 24); (b) simulated figure-of-merit ZT of GaN, $Al_{0.2}Ga_{0.8}N$, and $Al_{0.4}Ga_{0.6}N$ from 0 to 1000 K. The measured ZT values for $Al_{0.28}InN$ from Ref. 15 are indicated by stars.

The virtual-crystal model, which we adopted for GaN and verified experimentally,[23,24] qualifies for this task. Figure 6(a) shows the calculated thermal conductivity for GaN and two alloys, $Al_{0.2}GaN$ and $Al_{0.4}GaN$, from 0 to 1000 K, obtained with the virtual-crystal model. The details of the model can be found in Ref. 24. The prominent alloy-scattering effect on the thermal conductivity correctly reproduced by the model has been observed in the experimental studies.[23,24,37] The dependence of $Al_xGa_{1-x}N$ alloy thermal conductivity on Al mass fraction x is similar to that observed in $Al_xGa_{1-x}As$ (Ref. 38) and Si_xGe_{1-x} (Ref. 39) alloy systems.

Once both electron- and phonon-transport properties are modeled, the temperature-dependent ZT can be determined. Figure 6(b) shows the variation of ZT for GaN, $Al_{0.2}Ga_{0.8}N$, and $Al_{0.4}Ga_{0.6}N$ with temperature. The results are obtained for the moderate dislocation density $N_{dis} = 5 \times 10^8$ cm^{-2} in the crystal. The Al mass fraction is chosen below 0.4, which corresponds to the limit in most of the AlGaN barrier layers used in GaN/AlGaN heterostructure field-effect transistors (HFETs). However, it should be pointed out that the minimum phonon thermal conductivity in $Al_xGa_{1-x}N$ alloys is expected to be at $x \doteq 0.6$ (Ref. 24). The results of the simulations indicate that the $Al_xGa_{1-x}N$ alloy may have a relatively good ZT value at high temperature. The largest ZT, obtained for 1000 K, is about 0.2. This value, although lower than 1, is promising for practical application in spot cooling of GaN optoelectronic and power electronic devices. Since there is no experimental data available on the thermoelectric properties of $Al_xGa_{1-x}N$ at high temperature, we compare our results with the experimental data obtained for AlInN, a rather similar nitride alloy. The points indicated by stars in Fig. 6(b) are ZT values for the $Al_{0.28}In_{0.72}N$ alloy reported in Ref. 15. One can see that a good agreement is achieved, in both ZT values and their temperature dependence, between the measured data and our modeling results. The comparison indicates the accuracy of the model when the specifics in the electronic and thermal parameters of nitride semiconductors are taken into account.[35] It also adds some optimism to the prospects of improving the thermoelectric properties of GaN-based alloys.

The proposed model and simulation results suggest several possible approaches for further ZT improvement. One of them, related to the electron-transport optimization, is to reduce the extrinsic electron-scattering rates. As can be seen from the modeling results, in the heavily doped GaN materials the electron scattering on charged dislocations and ion-

Downloaded 25 Jun 2005 to 138.23.226.121. Redistribution subject to AIP license or copyright, see http://jap.aip.org/jap/copyright.jsp

ized impurities add significantly to the total scattering rate. The reduction of the dislocation scattering rate relies on the improvements of the material growth technology, which is expected to eliminate or significantly reduce the dislocations. For the ionized impurity scattering, removing dopants from the material is impractical because high doping is required in order to reach the optimum figure-of-merit.[14] The feasible approach for increasing μ_{imp} value is thus separating the donors (or acceptors) from electrons spatially, using the band-gap engineering and modulation-doping technology. For nitride materials, band-gap engineering and modulation doping are already used in HFET fabrication.[1–4] The application of the band-gap engineering for improving the thermoelectric properties of GaN/AlGaN heterostructures requires further investigation.

Another possible approach for *ZT* improvement in GaN-related materials is the thermal-conductivity reduction. In Fig. 6(b), the highest *ZT* value is obtained for $Al_{0.4}Ga_{0.6}N$, which has a thermal-conductivity value nearly five times smaller than that of bulk GaN. Further reduction of the thermal conductivity can be achieved by increasing the Al content to 0.6, as demonstrated in Ref. 24, or by adopting the quaternary alloying. Once the higher-quality GaN materials become available, one can achieve further reduction in k_{ph} through the phonon engineering approach.[40,41] Recent calculations carried out for wurtzite GaN-based heterostructures[42,43] indicate that the thermal conductivity can be varied in the acoustically mismatched planar heterostructures with the nanoscale layer thickness. A variation of this approach is to use the specially designed quantum-dot superlattices as thermoelectric material.[44] The experimental data indicate that the thermal conductivity can be reduced by more than an order of magnitude in the ordered nanostructured materials.[45] A simultaneous and correlated use of the electron band-gap[46] and phonon[41] engineering approaches may bring a significant *ZT* increase as the material's quality improves.

IV. SUMMARY

We carried out a detailed theoretical and computational study of the thermoelectric properties of wurtzite bulk GaN and related alloys. It was found that the room-temperature temperature *ZT* value for bulk crystalline GaN is about 0.0017. The *ZT* value can reach a value of 0.2 in the thermally resistive $Al_xGa_{1-x}N$ alloys at 1000 K temperature. Our calculated results are in good agreement with the available experimental data. The described model can be used to understand the effects of various electron-scattering terms on the thermoelectric properties of GaN. Based on the results of our calculations, we argue that GaN-based alloys can be potentially used as the high-temperature thermoelectric materials for the hot spot cooling in GaN optoelectronic and high-power electronic devices. Further improvement of the thermoelectric figure-of-merit in $Al_xGa_{1-x}N$ alloys can come from the improved control over the material's quality and the reduction of thermal conductivity using the phonon engineering approach.

ACKNOWLEDGMENT

This work was supported by the ONR Young Investigator Award to A.A.B. and the ONR award N00014-05-1-0150.

[1] U. K. Mishra, P. Parikh, and Y.-F. Wu, Proc. IEEE **90**, 1022 (2002).
[2] J. Li, S. J. Cai, G. Z. Pan, Y. L. Chen, C. P. Wen, and K. L. Wang, Electron. Lett. **37**, 196 (2001).
[3] H. Morkoc, *Nitride Semiconductor and Devices* (Springer, Berlin, 1999).
[4] Y. Wu, B. P. Keller, S. Keller, J. J. Xu, B. J. Thibeault, S. P. Denbaars, and U. K. Mishra, IEICE Trans. Electron. **E82-C**, 1895 (1999).
[5] O. Ambacher *et al.*, J. Appl. Phys. **87**, 334 (2000).
[6] R. Gaska, J. W. Yang, A. Osinsky, Q. Chen, M. A. Khan, A. O. Orlov, G. L. Snider, and M. S. Shur, Appl. Phys. Lett. **72**, 707 (1998).
[7] S. T. Sheppard, K. Doverspike, W. L. Pribble, S. T. Allen, J. W. Palmour, L. T. Kehis, and T. J. Jenkins, IEEE Electron Device Lett. **20**, 161 (1999).
[8] S. Keller, Y.-F. Wu, G. Parish, N. Zhang, J. J. Xu, B. P. Keller, S. P. DenBaars, and U. K. Mishra, IEEE Trans. Electron Devices **48**, 552 (2001).
[9] A. A. Balandin, S. V. Morozov, S. Cai, R. Li, K. L. Wang, G. Wijeratne, and C. R. Viswanathan, IEEE Trans. Microwave Theory Tech. **47**, 1413 (1999); A. A. Balandin, Electron. Lett. **36**, 912 (2000).
[10] S. L. Rumyantsev *et al.*, Semicond. Sci. Technol. **18**, 589 (2003).
[11] M. Kuball *et al.*, IEEE Electron Device Lett. **23**, 7 (2002).
[12] G. J. Snyder *et al.*, J. Appl. Phys. **92**, 1564 (2002).
[13] A. Yamamoto and S. Yamaguchi, Mater. Res. Soc. Symp. Proc. **793**, S8.24.1 (2004).
[14] S. Yamaguchi, Y. Iwamura, and A. Yamamoto, Appl. Phys. Lett. **82**, 2065 (2003).
[15] S. Yamaguchi, R. Izaki, K. Yamagiwa, K. Taki, Y. Iwamura, and A. Yamamoto, Appl. Phys. Lett. **83**, 5398 (2003).
[16] *CRC Handbook of Thermoelectrics*, edited by D. M. Rowe (CRC, Boca Raton, 1995).
[17] O. Katz, A. Horn, G. Bahir, and J. Salzman, IEEE Trans. Electron Devices **50**, 2002 (2003).
[18] N. G. Weimann, L. F. Eastman, D. Doppalapudi, H. M. Ng, and T. D. Moustakas, J. Appl. Phys. **83**, 3656 (1998).
[19] D. C. Look and J. R. Sizelove, Phys. Rev. Lett. **82**, 1237 (1999).
[20] W. Knap *et al.*, Appl. Phys. Lett. **80**, 1228 (2002).
[21] B. K. Ridley, B. E. Foutz, and L. F. Eastman, Phys. Rev. B **61**, 16862 (2000).
[22] J.-L. Farvacque and Z. Bougrioua, Phys. Rev. B **68**, 035335 (2003).
[23] W. L. Liu and A. A. Balandin, Appl. Phys. Lett. **85**, 5230 (2004).
[24] W. L. Liu and A. A. Balandin, J. Appl. Phys. **97**, 073710 (2005).
[25] B. R. Nag, *Electron Transport in Compound Semiconductors* (Springer, New York, (1980); N. W. Aschcroft and N. D. Mermin, *Solid State Physics* (Holt, Rinehart and Winston, Philadelphia, New York (1976).
[26] A. Balandin, S. Morozov, G. Wijeratne, S. J. Cai, R. Li, J. Li, K. L. Wang, *et al.*, Appl. Phys. Lett. **75**, 2064 (1999).
[27] J. Wang, R. Kaplan, H. K. Ng, K. Doverspike, D. K. Gaskill, T. Ikedo, I. Akasaki, and H. Amono, J. Appl. Phys. **79**, 8007 (1996).
[28] M. Luong and A. W. Shaw, Phys. Rev. B **4**, 2436 (1971).
[29] For example, B. K. Ridley, *Quantum Processes in Semiconductors*, 4th ed. (Oxford University Press, New York, 1982).
[30] W. G. Cady, *Piezoelectricity* (Dover, New York, 1964).
[31] J. Singh, *Physics of Semiconductors and their Heterostructures* (McGraw-Hill, New York, 1993).
[32] A. F. Ioffe, *Semiconductor Thermoelements and Thermoelectric Cooling* (Infosearch, London, 1956).
[33] D. Kotchetkov *et al.*, Appl. Phys. Lett. **79**, 4316 (2001).
[34] J. Zou *et al.*, J. Appl. Phys. **92**, 2534 (2002).
[35] *Properties of Advanced Semiconductor Materials GaN, AlN, InN, BN, SiC, SiGe*, edited by M. E. Levinshtein, S. L. Rumyantsev, and M. S. Shur (Wiley, New York, 2001).
[36] C. Shi, P. M. Asbeck, and E. T. Yu, Appl. Phys. Lett. **74**, 573 (1999).
[37] B. C. Daly, H. J. Maris, A. V. Numikko, M. Kuball, and J. Han, J. Appl. Phys. **92**, 3820 (2002).
[38] M. A. Afromowtz, J. Appl. Phys. **44**, 1292 (1973).
[39] H. Stohr and W. Klemm, Z. Anorg. Allg. Chem. **241**, 305 (1954).
[40] A. A. Balandin and K. L. Wang, Phys. Rev. B **58**, 1544 (1998).

Downloaded 25 Jun 2005 to 138.23.226.121. Redistribution subject to AIP license or copyright, see http://jap.aip.org/jap/copyright.jsp

[41] A. A. Balandin and K. L. Wang, J. Appl. Phys. **84**. 6149 (1998).
[42] E. P. Pokatilov, D. L. Nika, and A. A. Balandin, J. Appl. Phys. **95**, 5626 (2004); Superlattices Microstruct. **33**, 155 (2003).
[43] E. P. Pokatilov, D. L. Nika, and A. A. Balandin, Appl. Phys. Lett. **85**, 825 (2004).
[44] A. A. Balandin and O. L. Lazarenkova, Appl. Phys. Lett. **82**, 415 (2003).
[45] W. L. Liu *et al.*, J. Nanosci. Nanotechnol. **1**, 39 (2001).
[46] A. Casian, I. Sur, H. Scherrer, and Z. Dashevsky, Phys. Rev. B **61**, 15965 (2000).

Downloaded 25 Jun 2005 to 138.23.226.121. Redistribution subject to AIP license or copyright, see http://jap.aip.org/jap/copyright.jsp